Fermi National Accelerator Laboratory

FERMILAB-Pub-87/177-E
[E-741/CDF]

Calibration Systems for the CDF Central Electromagnetic Calorimeter*

S. R. Hahn, M. Miller, D. Connor, D. Bauer*, J. W. Cooper**,
R. Pierce, W. Mueller, R. VanBerg, and H. H. Williams
University of Pennsylvania
Philadelphia, Pennsylvania 19104 USA†

W. Li, L. Nodulman, J. Proudfoot, R. Rezmer,
D. Underwood, R. G. Wagner
Argonne National Laboratory
Argonne, Illinois 60439 USA‡

July-August 1987

*Submitted to Nucl. Instrm. Methods A

CALIBRATION SYSTEMS FOR THE CDF CENTRAL ELECTROMAGNETIC CALORIMETER

S.R. HAHN, M. MILLER, D. CONNOR, D. BAUER*, J.W. COOPER**,
R. PIERCE, W. MUELLER, R. VanBERG, and H.H. WILLIAMS
University of Pennsylvania, Philadelphia, Pennsylvania 19104 USA †

W. LI, L. NODULMAN, J. PROUDFOOT, R. REZMER,
D. UNDERWOOD, R.G. WAGNER
Argonne National Laboratory, Argonne, Illinois 60439 USA ‡

The central electromagnetic calorimeter for the Collider Detector at Fermilab was calibrated in a test beam of 50 GeV/c electrons. This calibration is maintained on long time scales with individual Cs^{137} sources for each module, and on short time scales with individual LED and xenon flasher systems on each module. The ratio of the 50 GeV/c electron response to the response to a Cs^{137} source is assumed to be constant; tests on the order of a month indicate a reproducibility of $\pm 0.4\%$. An average 2% loss of light yield over a period of 2 years has been observed.

---

*Work supported in part by the U.S. Department of Energy, Division of High Energy Physics, Contract DE-AC02-76-ERO-3071.

‡Work supported in part by the U.S. Department of Energy, Division of High Energy Physics, Contract W-31-109-ENG-38.

1.Introduction

In the Collider Detector at Fermilab[1], the successful calibration of the central electromagnetic (E-M) calorimeter[2] is critical for an understanding of events in the central region. The response of each detector module was first measured in a test stand using radioactive sources and cosmic rays[3]. Following this, the module's response to electrons and pions was studied in a test beam, making use of a movable fixture which allowed mapping as a function of position[4]. The calibration was determined at this time by directing a beam of 50 GeV/c electrons to the center of each tower; at nearly the same time, the response was measured with a permanently attached movable source and its associated drive for each module. The module's calibration was then tracked monthly with this same source after inclusion in the assembled detector[5]. Small changes in the energy response due to movement of the modules and from the magnetic field of the superconducting solenoid were accurately monitored. During physics running, this was supplemented by a fast calibration based on two flasher systems, one using LED's and one using a xenon flash tube, so as to maintain a daily calibration. Results of tracking the calibration over the course of the experiment thus far are summarized. Characteristics of the central E-M calorimetry calibration systems are summarized in Table 1.

The central E-M calorimeters' construction and the phototube specifications are given in References [2,6]. Each wedge module (Figure 1) is constructed in ten projective "towers" numbered 0–9. Tower 0 intercepts particles ejected at 90° to the direction of the beams (the 90° side); tower 9 is located on the 45° side. A module's "left" and "right" are defined as one's

left and right if one were facing an upright (as shown in the figure) module from the 90° side. Three calibration systems are associated with the central E-M calorimetry for each module. Each of the three systems is present in the form of a self-contained monitoring electronics package (Figure 2).

The three separate calibration systems offer complementary ways of injecting signals into the calorimeter before the phototubes. By using a source to inject a signal into the scintillator, a xenon flash to inject light into the waveshifter, and the green LED's to inject light into the phototube, each element of the system can be monitored for radiation damage or change due to aging or magnetic fields, and the calibration from the test beam can be retained during data taking. Furthermore, the gain of the phototubes can be measured from photo-statistics since the short term variation of the LED signal is very small. The merit of this approach was shown when it enabled an increase in source response, seen when the CDF solenoid magnet was energized, to be traced to an increase in scintillator light output as opposed to a change in photomultiplier gains. This is discussed in detail in section 8.

2.Source drive systems

Two source drive systems have been used for the central E-M calorimeter. The original calibration system was a 1 mCi Co^{60} source and associated motor driver which could be temporarily attached to a module for source runs. With this system, source runs could only be performed on one module at a time, and therefore, calibration of all 48 modules would have become a lengthy process. Furthermore, once the modules were placed in the assembled detector, the magnetic return yoke of the superconducting solenoid would not

allow room for attaching the Co^{60} motor driver. Thus, source calibrations would not be available during the data taking period. To reduce the time necessary for source calibration and to allow source runs during data taking runs, a second source drive system, consisting of a 3 mCi Cs^{137} source and drive hardware permanently attached to each module, was developed. This system requires less than an hour for E-M source runs on all modules, and, with proper beam conditions (no circulating beam or injection/extraction in the main ring), source calibration may be done during the data taking period. Further advantages of the Cs^{137} source are the long half-life of 30 years and low penetrating power such that the source in its lead housing does not degrade the adjoining hadron calorimeter; conversely, this source has the disadvantage that fewer scintillator layers of the calorimeter are sampled.

The Cs^{137} system was not developed prior to the calibration of the first 9 modules in the test beam; consequently, these modules were calibrated with Co^{60} and later cross calibrated to Cs^{137}. The Co^{60} source was also used to set the phototube high voltages for the 13 modules in the first test beam run. Thereafter, all source functions were performed by the Cs^{137} system. Details of the two systems are described below.

The source (whether Co^{60} or Cs^{137}) traverses the calorimeter between the eighth layer of lead and the ninth scintillator layer, near shower maximum. Its trajectory is determined by two parallel $\frac{3}{16}$ in. square cross section brass tubes which extend the length of the E-M calorimeter (along the beam direction). These two tubes are separated by $1\frac{1}{2}$ in. and are centered on the midline of the calorimeter; each is $93\frac{1}{2}$ in. long. The tubes are held in place by G-10 spacers and are incorporated into the construction of a strip

chamber (a gas wire chamber with cathode strip readout also located after the eighth layer of lead) which is utilized to determine the shower position. The tubes were terminated at the 90° end of the calorimeter at slots in a G-10 spacer. On the other side of this spacer, a $1\frac{1}{2}$ in. diameter brass pulley within a brass chock was aligned with the two slots. With the end and side plates of the calorimeter bolted in place, the open ends of the two brass tubes are accessible through two holes in the 45° end plate. Foam rubber inserts ensured mechanical stability and a good light seal around the exposed ends of these tubes.

The Co^{60} source was driven by a CAMAC-controlled stepper motor with position readback which could be bolted in place to the 45° end plate. The motor turns a steel drum with a grooved surface into which fits a cable which in turn enters the left tube, makes a 180° turn around the pulley at the far end, and exits the right tube to complete a loop back at the drum. On the left side, a 1 mCi Co^{60} source within a square capsule (which fit snugly in the tube) could be inserted into this loop of cable with brass clasps. This allowed the Co^{60} source to be driven anywhere from its garage to the G-10 spacer at the 90° end of the calorimeter. Its location was read back to within ± 2 mm; the limit of travel was located slightly beyond the middle of the tower closest to 90° (tower 0).

A permanent Cs^{137} source system was mounted to the 45° end plate following Co^{60} system tests for the first 13 wedges and initially for the remaining wedges. This source drive services both the E-M and hadron calorimeters. The drive mechanics are constrained to lie on the surface of a module's end plate and can protrude no more than $1\frac{1}{2}$ in. from it due to the limited amount

of space between the module and the magnetic return yoke of the solenoid in the assembled detector. Thus, a system with position readback was abandoned as impractical. Instead, a system was developed which recorded the current of each phototube at 0.3 second intervals as the source moved at a constant speed. Subsequently, the current channel's profile for each tower was fit to determine the peak current.

During construction of the modules, a tube and pulley system similiar to that already described for the E-M calorimeter was built into the hadron calorimeter. This consisted of two parallel 0.109 in. OD brass tubes aligned with a pulley which was fastened between two plates. A bolt attached to the plates extends through the 90° end plate of the calorimeter. The open ends of the brass tubes are flared so as to be held in place in the 45° end plate and to keep them in the proper location. Tension was applied to the tubes to straighten them. The tubes are located $1\frac{1}{2}$ in. apart centered on the midline of the hadron calorimeter between the seventh scintillator layer and the seventh steel plate in the stack. During installation of the Cs^{137} system, 0.109 in. OD stainless steel tubes with surrounding spacers were also placed in the square brass tubes in the E-M calorimeter. These ensured that the 0.063 in. OD Cs^{137} source capsule, which was smaller than the Co^{60} source capsule, would be constrained transverse to the direction of travel within the 0.085 in. ID of the tubes.

The mechanical portions of the Cs^{137} source drive system were mounted on two plates that were bolted to the 45° end plate of the calorimeter (Figure 3). The bottom plate is mounted on the E-M calorimeter and contains four Delrin pulleys which guide the cable (and source) into the two tubes

in the E-M calorimeter. The top plate, which is mounted on the hadron calorimeter, contains the majority of the hardware. On this plate, another four Delrin pulleys are configured like the E-M plate to guide the cable through the two tubes into the hadron calorimeter. A drive pulley is connected through a geared drive belt to the drive motor, and a tensioning pulley holds the cable under the proper tension to make good contact with the drive pulley. Also on the hadron plate are a series of limit switches described below, and a lead housing where the source was normally located except during source calibration runs. An anodized aluminum coverplate covers all this hardware except a portion of the drive belt which runs between the motor and the drive pulley, and the motor itself. A small, low voltage motor with attached permanent gearbox (Portescap $\frac{7}{8}$ in. dia. escap D.C. motor 210E with 190:1 reduction gearbox R22) was employed to ensure constant speed of the source. After installation of the drive hardware, a complete loop of nylon-clad 0.019 in. dia. stainless steel cable was installed. The cable enters the hadron calorimeter, goes around the pulley at the other side of the calorimeter, comes out next to where it entered, is threaded through the limit switches and pulleys, enters the E-M calorimeter to again travel the length of the calorimeter and return, and is threaded through the tensioning, idler, and drive pulleys back on itself to form a loop. The loop was completed by the cable ends being tied onto a brass capsule containing the Cs^{137} source (average activity for 51 sources of 3.12 ± 0.09 mCi with half-life of 30.01 years, due to admixture of other isotopes). The tension on the tensioning pulley was adjusted to provide smoothest operation.

A system of limit switches was used to prevent the source capsule from

going around the pulley in the hadron calorimeter or from hitting the G-10 spacer in the E-M calorimeter. The position limits are determined by portions of the cable from which the nylon cladding has been stripped. The limit switches (see Figure 3) are brass rollers on stainless steel leafs mounted on each side of the cable. Electrical contact is made when the bare strip on the cable is located between the rollers. The three pairs of switches from top to bottom are denoted "hadron", "garage", and "E-M". The "garage" location, with the source capsule centered in the lead housing, is indicated by continuity at only the "garage" contact (due to a short bare spot on the cable). The "hadron" limit, at which travel into the hadron calorimeter ceases, is indicated by continuity at both the "garage" and "hadron" switches due to a long bare spot on the cable; the "E-M" limit is handled similiarly. Control of the drive motor and limit switch functions are handled by the calibration control RABBIT card discussed later.

Operation of the source drives is controlled by several programs. The standard CDF data acquisition program[7] is used to read out the current channels on all 48 modules simultaneously via the RABBIT system[8]. Another program allows real-time control of the drive motor and readback status of the limits. Yet another program samples the data stream so as to provide a real-time plot of every module's current channel activity. Figure 4 displays the plot from a single module containing a current channel peak for each module tower (from the sum of the two photomultipliers signals which view that tower).

3. The xenon flash system

To inject light into the waveshifter, an optical fiber is inserted into a hole in the acrylic prism glued to the transverse edge of each waveshifter. The single quartz fibers glued into the prism for each waveshifter are bundled together and illuminated by the xenon flasher for each module; a disassembled xenon flasher is shown in Figure 5. The trigger signal generated in the calibration control card passes through a pulse shaping circuit in the xenon flash box and subsequently switches a HV FET, causing the bulb to fire. The scintillator rod absorbs the light and re-emits it into the bundled quartz light fibers and the 3 monitoring PIN diodes. The resulting charge in the phototubes is integrated and read out through the photomultiplier amplifier RABBIT card. The PIN diode signals are pre-amplified in the xenon flash box, then read out through sample-and-hold circuits on the calibration control card. In addition, time-to-voltage circuits on the calibration control card measure the time of each of the PIN diode signals (Figure 6).

The xenon flash bulb contains two main electrodes, a trigger electrode, and a pre-ionizing electrode. In normal operation first the pre-ionizing electrode discharges, then the trigger electrode discharges, and finally the main electrodes break down, thereby resulting in a large pulse of light. The time jitter associated with this mode of operation is too large for our purposes; superior operation was obtained for direct discharges from the trigger electrode to one of the main electrodes (the other electrode was left floating). The light amplitude is sufficient and the jitter is significantly reduced. Bulb performance varied considerably when operated with the modified trigger circuit; therefore, bulbs which exhibited unstable discharges or had large

timing jitter were rejected. Typical jitter for accepted bulbs is 15 ns. The PIN diodes are relatively insensitive to temperature, exhibiting an average temperature coefficient of $-0.06\%/^{\circ}C$. The ratio of any 2 PIN diode signals from a single flasher boxes yields an average sigma of 0.23%. The rise time of the flasher pulse is 120 ns and 99% of the integrated charge is readout from the PIN diode pre-amplifiers in less than 1 μs.

4.The LED flash system

To monitor the response of the photomultipliers themselves, an LED (light emitting diode) system injected light almost directly into the photomultipliers. Two 0.6 mm diameter quartz optical fibers (one used and one spare) are glued into two mounting holes constructed into the rectangular-to-round transition piece fronting each phototube. The other end of the used fiber is terminated at an optical connector fastened to an optical output on the LED flasher system.

Each calorimeter module has a box containing three green LED's, 8 fan-out fibers from each LED, two PIN diodes for reference, electronics for driving the LED's, and charge sensitive pre-amplifiers for the PIN diodes. Ideally, one would like to feed fibers to all the phototubes and reference diodes from a single LED. This was not possible because of the variation in light going into each fiber if more than 8 fibers are coupled to a single LED. Therefore, it was necessary to utilize 3 LED's. Normally, each of the three LED's is flashed in sequence, with digital bits set in the calibration control card indicating which LED should have fired. The light output of two of the LED's (LED0 and LED2) are monitored directly by PIN diodes. The output of the

third (LED1) is monitored indirectly by the PIN diodes; one photomultiplier views LED0 and LED1 (fired successively), and another photomultiplier views LED1 and LED2.

The light output of the LED's is temperature sensitive, with an average temperature coefficient of $-0.5\%/°C$. The temperature of each box is monitored with a temperature probe, as are several phototubes in the calorimeter and two internal locations within the scintillator stack. The LED's are run with a capacitor discharge system using a DAC controlled voltage with a maximum of 13.5 V. The rise time of the light output is 70 ns and the fall time is also 70 ns. A long tail in light output after the FET switch is shut off is eliminated with resistors in parallel with the LED's (Figure 7).

5.The calibration control card

All the calibration systems for the E-M calorimetry are controlled by, and read out with, a card within the RABBIT[8] front-end electronics system. This system employs two redundant multiplexed analog buses and an eight bit wide digital bus; the calibration control card uses both buses to read out analog data and to receive digital commands and read out digital status information. Figure 8 summarizes the functions of the calibration control card. One concern associated with the xenon flash and LED systems is that the rate at which the timing gates were sent (typically a complete timing cycle takes 7.0 μs) is faster than the regeneration times of the flashers (hundreds of μs). Countdown circuitry was included in the design of the calibration control card to deal with this problem: this circuitry counted down from a digitally loaded value the number of timing gates sent to the card from the

BAT, the RABBIT card which converts beam timing gates into the necessary gates on the RABBIT backplane for readout of analog sampled data. After the required number of transitions, the calibration control card produces a trigger signal for the selected flasher system, and sends a trigger signal out through a front panel ECL connector.

6. Test beam measurements

Fifty wedge modules were constructed — 48 modules in the detector and 2 spare modules for backup and testing. These modules were calibrated in the NW test beam at Fermilab. The electromagnetic calibration consisted of runs with 50 GeV/c electrons and a series of source runs taken immediately before or after each electron run. We attempted to take 2 or more electron runs with their associated source runs on each module to help determine the accuracy of the calibration and to help eliminate bad data; however, time limitations prevented our repeating the measurements on 12 modules. Typically, the calibrations were taken within a span of 2 days.

Electron runs consisted of a 50 GeV/c electron beam incident on tower center for 9 of the 10 towers in the module. Tower 9 at the 45° end of the module has a significantly different geometry and fewer radiation lengths than the other towers. Electron scans were used to determine the beam position which maximized the phototube response for this tower, and that position was chosen for the electron calibration.

Several cuts were made by the online data acquisition program[7] on the electron events. Using position information from the strip chamber embedded at shower maximum in the module, electrons were required to be within

1 cm of tower center in the x direction (Figure 1). This cut ensured equal energy sharing by the 2 phototubes collecting light from each tower. The electron momentum was determined by 2 beam chambers on either side of a dipole bending magnet (Figure 9). If the online program was unable to reconstruct the particle momentum from the beam chamber data, the event was discarded. The momentum was used to scale all events to 50 GeV/c. Timing information from the scintillator trigger counters was used to reject events with more than one particle contributing signal during charge integration.

The photomultiplier gains were set to give 100,000 fC per phototube for a 50 GeV/c electron incident on that phototube's tower center. About 200 good events per tower were recorded for calibration runs, yielding a statistical error in the calibration value, fC/(50 GeV), of roughly 0.15% (the E-M calorimeter has an energy resolution of $\sigma/E = 13.5\%/\sqrt{E \sin\theta}$ with E in GeV; see [2]). The systematic error due to mismeasurement of the electron beam momentum was $\pm$0.3%. Sources of this error were the error in the magnetic field measurement, and the error in the beam chamber survey. Errors due to uncertainties in the gains of the integrated charge channels measuring the energy response and the current channels measuring the source response were less than 0.25% and 0.15%, respectively. The major source of the error on the charge channels was the systematic uncertainty in the charge injection capacitor's value. The major source of the error on the current channels was the statistical error in the gain measurement. These gains were measured in a test RABBIT crate with associated gating logic, using a linear fit to input pulses or currents over the dynamic range of the

photomultiplier amplifier card.

As mentioned earlier, the first 9 modules were calibrated with Co^{60} before being converted to permanent Cs^{137} drives. For these modules, the Co^{60} motor driver accurately positioned the source at the center of each tower, and the phototube current was read with a picoammeter. Only one Co^{60} run was taken for each electron run. The peak current was roughly 100 nA per phototube. Later, these modules were cross-calibrated to the Cs^{137} source drives. This procedure consisted of taking four Co^{60} runs, installing the permanent Cs^{137} drives, and taking four Cs^{137} runs. Using the ratio of the means of these runs for each tower and accounting for the decay of the Co^{60} source from the original calibration runs, allowed us to carry the calibration over to the Cs^{137} system.

To obtain consistent and reliable data, typically 4-6 Cs^{137} source runs were taken per electron calibration run. The averages of these runs were calculated to form a single source calibration value for each channel. The peak current using Cs^{137} is roughly 50 nA per phototube.

As will be shown below, the source current reproducibility for an average channel for Cs^{137} runs is $\pm 0.4\%$. The error for channels originally calibrated with Co^{60} has two components — the error in reading the picoammeter and the error in the process of converting the calibration to Cs^{137}. These channels have a combined average source current error of about $\pm 0.9\%$.

7.Calibration measurements

In normal physics runs, the MX front-end scanners control the readout of the charge-integrating channels for the calorimeters—for each channel, a pedestal

is subtracted, and the result digitized and stored only if larger than a threshold. Before being read out, each digitized channel is multiplied by its corresponding calibration constant which corrects for channel-to-channel gain variation. These constants are divided by a nominal value (such that they are near unity); hence one retains as much of the original 16-bit dynamic range of the ADC as possible. All digitized channels can then be converted to units of energy by multiplying by the one nominal value.

The channel-to-channel variations in the response of the calorimeter to a pulsed deposition of energy is tracked as a function of time by measurements of the response to the Cs^{137} source. It has been verified that the pulse response (integreted charge Q) measured by the charge-integrating channels remains proportional to the Cs^{137} source peak (current I) measured by the current channel on the same photomultiplier. Thus, for the test beam at time t_0 and a later time t:

$$\frac{Q(t)}{I(t)} = \frac{Q(t_0)}{I(t_0)}$$

The energy gain G_E for a particular phototube (in GeV/count) can then be derived from the energy gain calculated in the test beam at time t_0, taking into account the peak source current measurements I (in nA) and the measured charge channel electronic gains G_Q (in fC/count):

$$G_E(t) = \frac{G_Q(t)}{G_Q(t_0)} \frac{I(t_0)}{I(t)} G_E(t_0)$$

The source current terms contain the current channel electronic gain G_I (in nA/count) and a correction factor for the radioactive decay of the source. The dimensionless channel-to-channel variation G'_E is defined in terms of the

energy gain G_E (in GeV/count) and a nominal energy gain:

$$G'_E(t) = \frac{G_E(t)}{G_E(\text{nominal})}$$

Short-term corrections from the time of the last source calibration t_1 can be made with one of the flasher systems' signals Q_f, assuming $G_Q(t) = G_Q(t_1)$:

$$G_E(t) = \frac{Q_f(t_1)}{Q_f(t)} G_E(t_1)$$

One would prefer to use a signal Q_f with as small a statistical error as possible. As will be shown in the next section, this proved to be the ratio of phototube signal to PIN diode signal for the xenon flasher and the phototube signal itself for the LED flasher. In practice, the constants are not a continuous function of time, but are measured at discrete intervals: from 2-4 weeks for the source measurements, and daily for the flasher measurements. Convenient rearrangements of the values used in the above equations—$[Q(t_0)/E(t_0)]/I(t_0)$, $G_Q(t)$, and $I(t)$—are stored in a calibration data base, and retrieved to form values $G'_E(t)$ which are also stored in the data base for downloading to the MX front-end scanners.

8.Performance

A typical distribution of the percentage difference between the results of two source runs (Figure 10), one with the Cs^{137} source entering the 45° end plate and traveling from tower 9 to tower 0, the other with the source run in the opposite direction, has a mean and rms of $(0.02 \pm 0.61)\%$. The results from all 956 phototubes in the central E-M calorimetry [9] are included in this comparison, except for a few channels for which the source peak fits fail due

to noise spikes from cosmic rays or electronic noise.

The distribution of pulse heights produced by the xenon flash has a broad peak due to the variation in the xenon flash bulb's output from event to event. Typically, its mean value corresponds to a particle of 20-40 GeV; in Figure 11a, the mean and rms are 5510 ± 896 counts which corresponds to 31.5 GeV. The xenon flash intensity is monitored by temperature-stable PIN diodes; the PIN diode distribution for the xenon flash for the same flasher run is shown in Figure 11b with mean and rms of 21800 ± 3470 counts. To obtain the phototube response normalized to a fixed light intensity, the phototube signal is divided by the sum of the three monitor PIN diode signals (and multiplied by a factor of 10000 so as to avoid fractions). The event-by-event distribution of this ratio is shown in Figure 11c for the same phototube; the mean and rms are 8040 ± 160. Note that the PIN diodes have divided out the typical two-peaked distribution in the raw phototube distribution and lowered the fractional rms from 16% for the unnormalized distribution to 2%. The ratio of 2 PIN diode signals typically has an rms near 0.2%. When the flasher runs are analyzed, both pedestal-subtracted phototube ADC counts and ratios of the phototube signal to the appropriate PIN diode signal are stored in the calibration database.

The LED produces a narrow phototube peak typically corresponding to a particle of 200–300 GeV with a fractional rms on the order of 0.8%. For the LED's, the normalization used depends on the phototube in question. A group of 7 phototubes views a single LED (LED0) which is monitored by a single PIN diode. A second group of 7 phototubes is flashed and monitored by another LED (LED2) and PIN diode. The remaining 6 phototubes, plus

one phototube from each of the first two groups, are flashed by yet another LED (LED1). Since one phototube is successively illuminated by LED0 and LED1, and another phototube is successively illuminated by LED1 and LED2, the normalization of LED1 may be obtained even though it is not viewed directly by a PIN diode. The LED phototube distribution is so narrow that dividing the phototube signal by the PIN diode increases the fractional rms only slightly less than the statistical sum of the phototube signal rms and the PIN diode signal rms.

Figures 12a and 12b show percentage differences between two xenon flash runs and two LED runs separated by a short period of time (about one day); the phototube outputs have been normalized to the PIN diodes for the xenon data while the raw differences are shown for the LED's. Since the phototube stability has been good, we have used the flashers only to correct coherent effects over groups of phototubes.

Figure 13 exhibits trends seen in source measurements over a period of time corresponding to about 9 months. Approximately 90% of the phototubes show a flat distribution demonstrating no change in the source response over that period of time, some show gradual shifts up or down, and some show abrupt shifts in source response. The primary source of these variations is changes in the photomultiplier gains, either intrinsic changes in the phototubes themselves or changes in the high voltage supplied to the phototube base.

Figure 14 illustrates the long-term variations for the xenon flash and LED systems; the variations are typically of order a few percent and the two systems generally track one another. These systems are intended primarily

for short-term corrections, and large shifts are carefully verified before use as corrections.

An interesting effect that has been observed is an increase in the Cs^{137} source response in the E-M calorimeter when the CDF superconducting solenoid[10] is activated (Figure 15). A simple 2-D axisymmetric model of the magnetic field throughout the detector predicts a field in the E-M calorimeter mostly parallel to the plane of the scintillator layers varying from 120 gauss in the middle of the calorimeter to more than 860 gauss in portions of tower 9 and a field of 20–40 gauss over most of the top of the wedge module in the vicinity of the phototubes. The iron and mu-metal shields surrounding the E-M phototubes should easily shield this magnetic field. The increase in source response varies from tower to tower, decreasing away from towers 0 and 9, and from module to module. On the other hand, no change is seen in the LED response; since the LED light signal is injected via light fibers just below the photocathode, these two results indicate an intrinsic change in the scintillator light output. This increase in scintillator response to ionizing radiation as a scalar function of magnetic field has been seen in other organic scintillators[11] and is a well-known phenomenon of these scintillator's organic chemistry. This change in calorimeter response should be automatically accounted for in the calibration constants.

Over the course of more than a year, several source drive motors have failed to operate in the nominal magnetic field. We also measure responses with the field off, in which case all the motors work. We correct by an overall factor those modules whose motors do not work with the field on (these corrections range from 0.0% to 2.0%).

Energy calibration corrections are predicated on the ratio of the electron energy response to the source response being a constant. In the test beam run, three modules (one module on two occasions) were recalibrated in the test beam roughly one month after the original calibration, sometimes after deliberately attempting to change the electron response by rotating the wedge module into an inverted position. Between calibrations, these modules were transported to a storage site. Figure 16 shows the percent difference in the ratio of electron response to source response between the two measurements; taking into account that each point actually represents two measurements, the reproducibility corresponds to an error of $\pm 0.4\%$, and the change of 0.2% seen is just the loss expected from radioactive decay.

It is also desirable to have a uniform source response (and thus energy response) throughout the calorimeter. In addition to the charge integrating and current channels on each RABBIT photomultiplier amplifier card, there are "fast out" triggering channels connected to the the charge integration circuitry. Uniform response simplifies triggering using these outputs, as well as maximizing the dynamic range overall. Figure 17a shows a recent distribution of channel-to-channel gain variations with mean and rms of 1.03 ± 0.08; this demonstrates uniformity, dominated by the reproducibility of setting phototube high voltages, of 8% and an intrinsic deterioration of response due to aging over the course of two years. Figure 17b shows the same distribution as Figure 17a but for the original calibrations done in the test beam and Figure 18 shows the percentage change between the two sets of energy responses. This last plot shows the actual changes in energy response from the test beam (1984–1985) till the most current set of source

runs (May 1987).

9.Conclusions

In summary, we have implemented a set of calibration systems which should allow relative normalization of individual tower energies to $\pm 0.4\%$ with absolute normalization referenced to 50 GeV/c test beam electrons. Systematic studies of colliding beam data will be used to confirm this performance.

We gratefully acknowledge the support of our colleagues on CDF, members of the University of Pennsylvania and Argonne technical staffs, the CDF experimental support group, and Fermilab experimental operations crew. This work was supported in part by the U.S. Department of Energy.

* Present Address: University of California, Santa Barbara, Santa Barbara, California 93106 USA

** Present Address: Fermi National Accelerator Laboratory, Batavia, Illinois 60510 USA

References

[1] *The Collider Detector at Fermilab*, F. Abe et al., submitted to Nucl. Inst. and Meth.

[2] *The CDF Central Electromagnetic Calorimeter*, L. Balka et al., submitted to Nucl. Inst. and Meth.

[3] *Cosmic Ray Test of the CDF Central Calorimeters*, R.G. Wagner et al., submitted to Nucl. Inst. and Meth.

[4] *Response Maps of the CDF Central Electromagnetic Calorimeter*, K. Yasuoka et al., submitted to Nucl. Inst. and Meth.

[5] S. Hahn et al., proc. DPF at Santa Fe (1984) 365.

[6] *Phototube Testing for CDF*, T. Devlin et al., submitted to Nucl. Inst. and Meth.

[7] D. Quarrie, IEEE Trans. Nucl. Sci. **32** (1985) 1467.

[8] G. Drake et al., IEEE Trans. Nucl. Sci. **33** (1986) 92;
G. Drake et al., IEEE Trans. Nucl. Sci. **33** (1986) 893
Front End Electronics: The RABBIT System, G. Drake et al., submitted to Nucl. Inst. and Meth.

[9] The "chimney" wedge module is a single special module constructed so as to allow access to the CDF superconducting solenoid magnet. The E-M calorimeter in this module consists of normal towers 0–6 and a tower 7 which combines the area of the normal towers 7 and 8. There is no tower 9 in this module. Therefore, there are a total of 956 phototubes (48 wedge modules, each with 10 towers containing 2 phototubes, less 4 phototubes not present in the "chimney" wedge module) in the central E-M calorimetry. See also Reference [2].

[10] H. Minuemura et al., *Construction and Testing of a* 3 $m \times 5$ m *Superconducting Solenoid for the Fermilab Collider Detector Facility (CDF)*, NIM in Physics Research **A238** (1985) 18.

[11] C. Swenberg and N.E. Geactinov in: Organic Molecular Photophysics.,

J.Birks, ed. (J. Wiley and Sons, New York, 1973) vol. 1;

S. Bertolucci et al., Nucl. Inst. and Meth. **254** (1987) 561.

Table 1: Central Electromagnetic Calorimetry Calibration Systems Summary.

Global parameters		
	Reproducibility specification	better than 1%
	One set of systems per module	50 (12/arch + 2 spare)
Cs^{137} source drive system		
	Radioactive source	3 mCi Cs^{137} encapsulated
	Depth (from interaction region)	$5.9X_0$ (shower maximum)
	Motor	190:1 gear ratio; nominal D.C. voltage 3.5 V
	Normal source speed	$\frac{2}{3}$ cm/sec
	Normal data rate	3–5 Hz
	Source peak fitting algorithm	6th-order polynomial fit to top 20% of peak with maximum found by Newton's method
	Typical peak value (when source decay is compensated)	50.0 ± 0.2 nA
Xenon flash system		
	Light distribution	Xenon flash bulb illuminating scintillator in turn illuminating 20 quartz light fibers and 3 PIN diodes; light fibers enter each waveshifter through prism
	Light pulse characteristics	100 ns rise time; 100 ns fall time
	Regeneration time	< 10 ms
	Jitter from trigger to pulse	±15 ns
LED flash system		
	Light distribution	3 LEDs—2 of 3 illuminate 7 light fibers and one PIN diode each; remaining LED illuminates 8 light fibers, two of which share another LED for purposes of cross-calibration. Light fibers enter transition piece directly below phototubes.
	Light pulse characteristics	50 ns rise time; 50 ns fall time
	Regeneration time	< 1 ms
	Jitter from trigger to pulse	±5 ns
Performance		
	Short-term (< day) reproducibility	±0.3%
	Long-term (≈ month) reproducibility	±0.4%
	Original uniformity of energy response	±4.0%
	Current energy response mean and rms normalized to nominal	1.03 ± 0.08

Figure captions

1. Schematic of a wedge module of the CDF central calorimeter showing the coordinate system as measured by the strip chamber used for test beam energy and mapping measurements. The 45° end plate is in the $+z$ direction; the "left" of the module was defined as being in the $+x$ direction.

2. Relations between the calibration systems and the calorimeter response for the central electromagnetic calorimetry.

3. Photograph the layout of the Cs^{137} source drive located on the 45° end plate of a central wedge module. The central E-M calorimeter is located under the bolted aluminum plate; the central hadron calorimeter is located beneath the black steel above the E-M calorimeter. The mechanical portions of the source drive are bolted in two sections; the 3 mCi source is located in the lead housing beneath the small radioactivity warning sign.

4. Typical output of the real-time source monitoring program showing sums of photomultiplier current readouts as a Cs^{137} source travels at a constant rate through a wedge module. In typical running, all 48 module's plots were displayed simultaneously. The sum of all current channels in the even towers (with two phototubes per tower) is shown as one trace, and the sum of all odd towers, as another trace. The plot of current channel ADC counts for a *single* phototube is mostly dark current with a single peak when the source enters and passes through that phototube's tower.

5. Photograph of dismantled xenon flasher showing light-tight construction, electronics, xenon flash bulb, scintillator rod, and PIN diodes.

6. Circuit diagrams of electronics in the xenon flasher: (a) the high voltage triggering circuit to fire the xenon flash bulb, and (b) the PIN diode pre-amplifier circuit.

7. Circuit diagram of the LED triggering circuit in the LED box; the PIN diode pre-amplifier circuit is similiar to that in the xenon flasher. The major differences are: the feedback capacitance is 1 pF instead of 26 pF, the PIN diode used is a BPX65, the FET utilized is a E110, the bias voltages are ± 6 V, and the output coupling capacitors are .47 μF.

8. Block diagram of calibration card functions.

9. Schematic of the NW test beam line with beamline momentum analyzing beam chambers and dipole.

10. Comparison of two Cs^{137} source runs, one immediately after another. Shown is the distribution of percentage differences defined as (Run2 − Run1)/Run1 × 100%.

11. Typical distributions of results from xenon flash runs. (a) Distribution of raw phototube signals (in ADC counts) seen during xenon flash runs. (b) Distribution of PIN diode signals (in ADC counts) seen during xenon flash runs. (c) Distribution of ratios of raw phototube signals

to PIN diode signals (in dimensionless units) for xenon flash runs. See the text for details of how these ratios are calculated.

12. Comparisons of two xenon flash and LED runs separated by about a day. For the xenon flash, the ratio of raw phototube signal to PIN diode signal was compared; while for the LED's, the raw phototube signal was used.

13. Some typical long-term variations in source response over a period of about nine months. For 95% of the phototubes, the variation in response was flat (a); in a small number of cases, the response fell (b) or rose (c) or an abrupt change was seen (d).

14. Some typical long-term variations in xenon flash and LED response over a period of about three months.

15. Percent change in Cs^{137} source response as a function of the CDF superconducting solenoid field (nominal field is 15 kG).

16. Calibration reproducibility. The difference in beam to Cs^{137} source ratio for each tube is plotted for successive calibration procedures, about 5 weeks apart, for three modules. The deviation of the centroid from zero corresponds accurately to the source decay.

17. Calibration uniformity. A recent distribution (May 1987) of channel-to-channel energy response gain variations for all central E-M calorimeter channels (a) demonstrates good uniformity in energy response. A distribution of the same quantity is also shown as measured from the test beam calibration (b).

18. Percentage difference between current (May 1987) calibration and the original test beam calibration for the energy response.

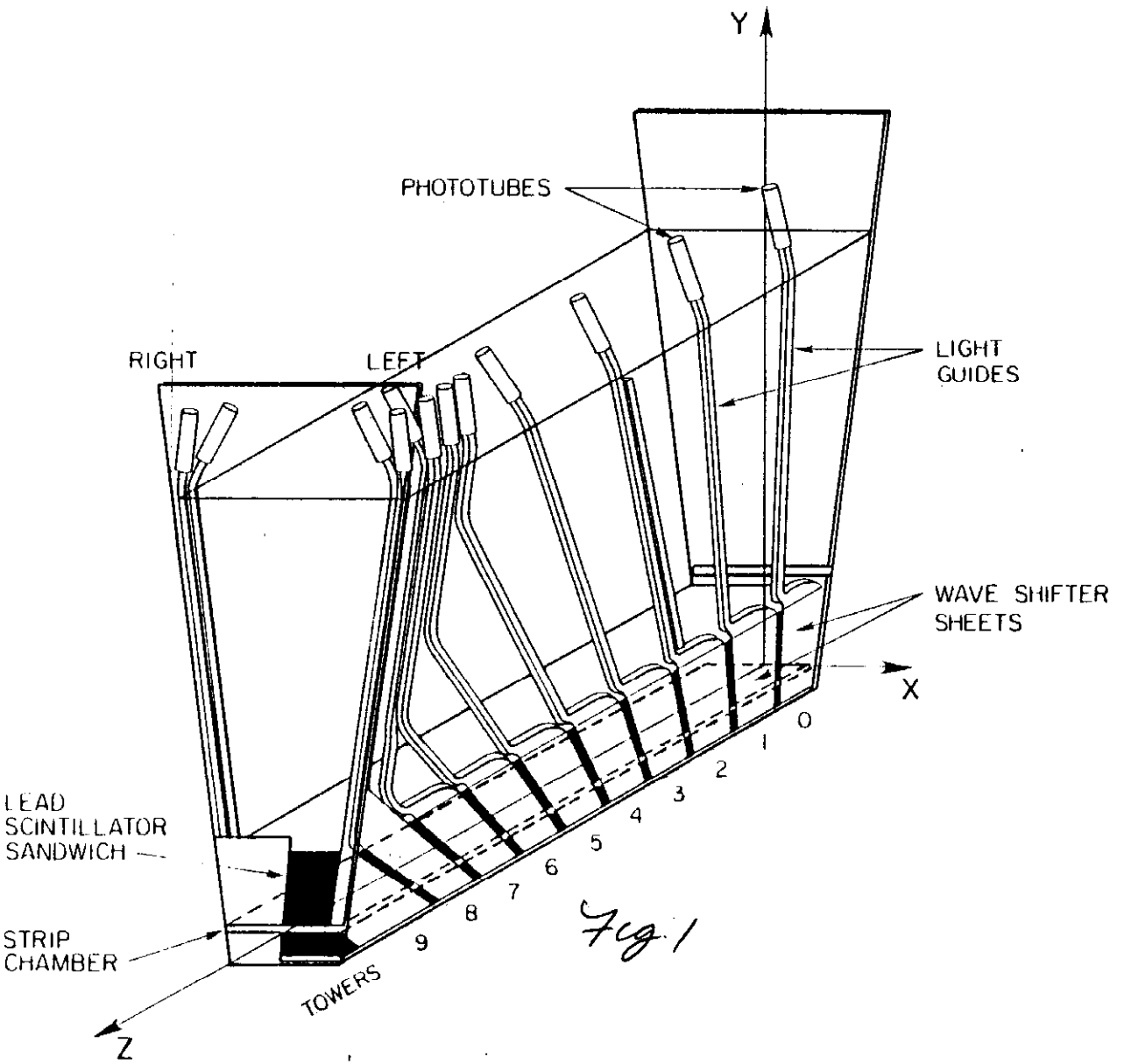
Y
PHOTOTUBES
RIGHT
LEFT
LIGHT
GUIDES
WAVE SHIFTER
SHEETS
X
0
1
2
3
4
5
6
7
8
9
TOWERS
LEAD
SCINTILLATOR
SANDWICH
STRIP
CHAMBER
Z

Fig. 1

CDF Central E-M Calorimeter Calibration Systems

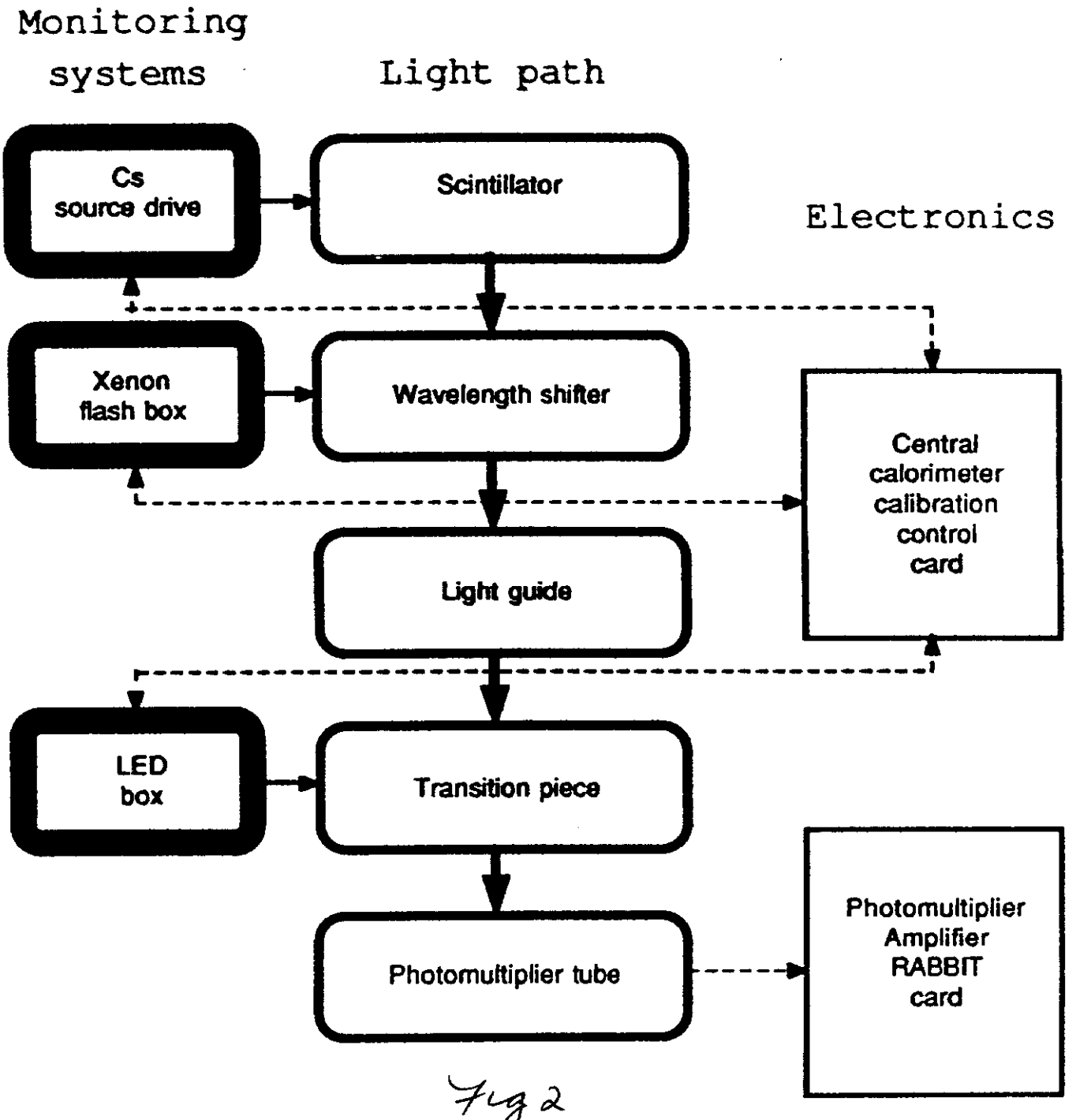

Fig 2

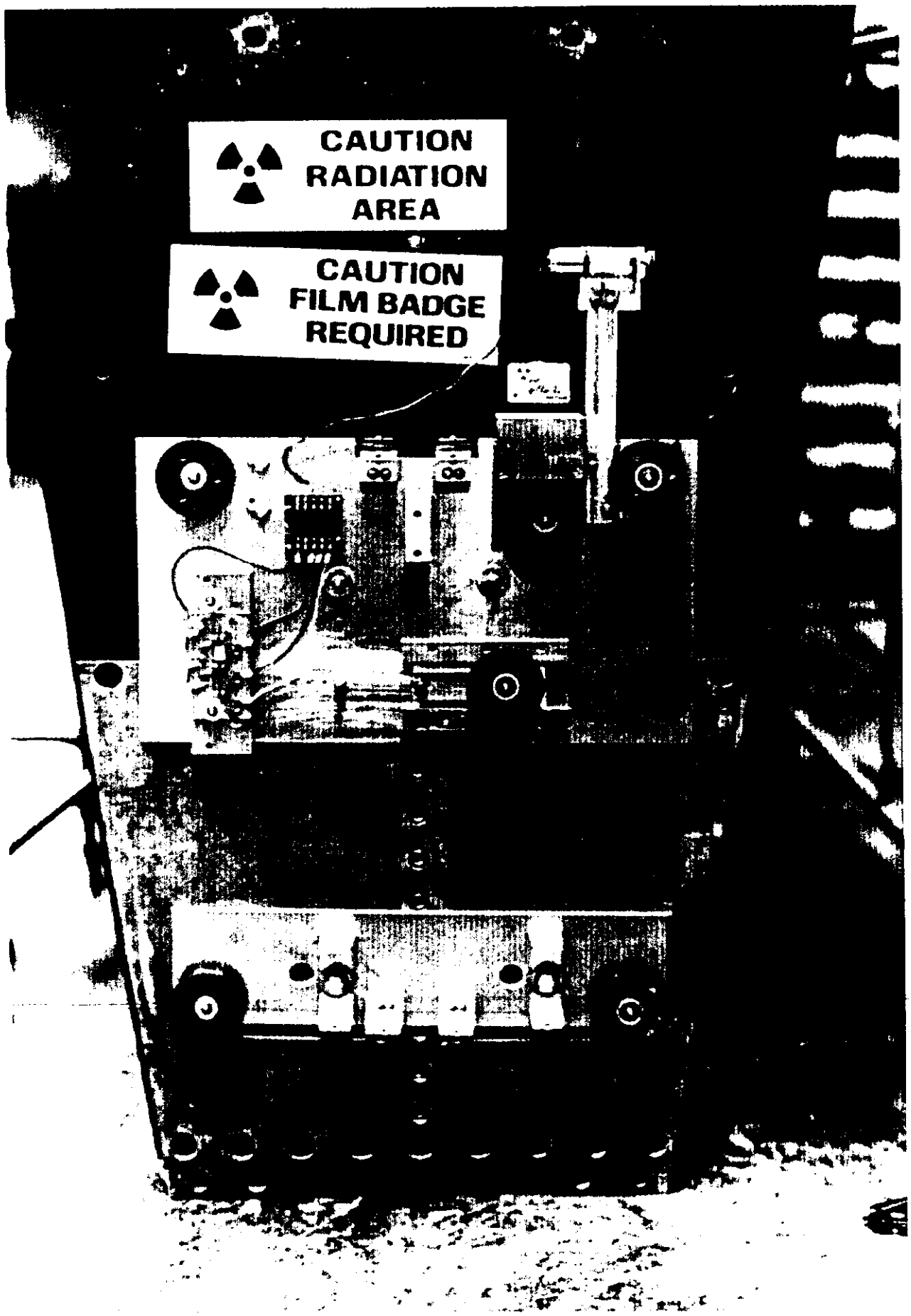

Fig. 3

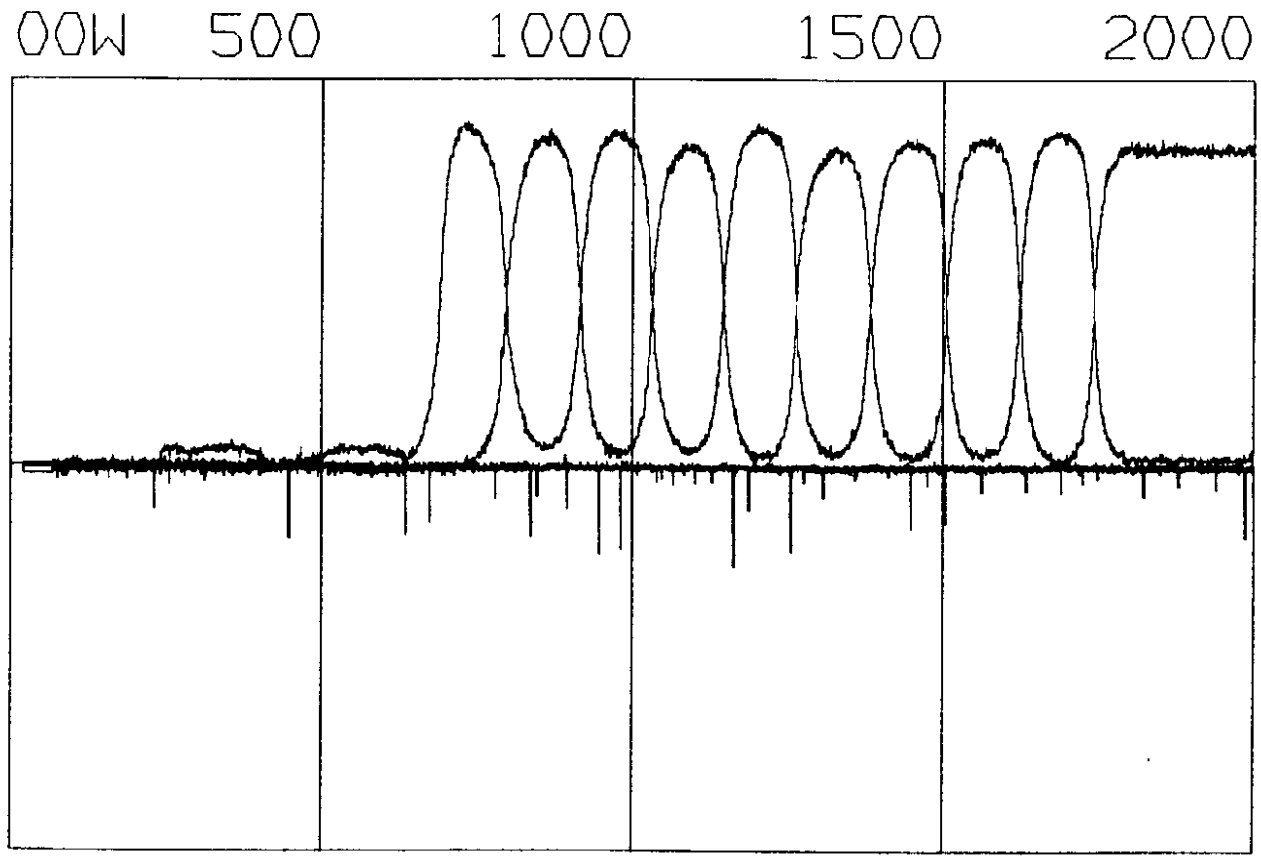

Fig. 4

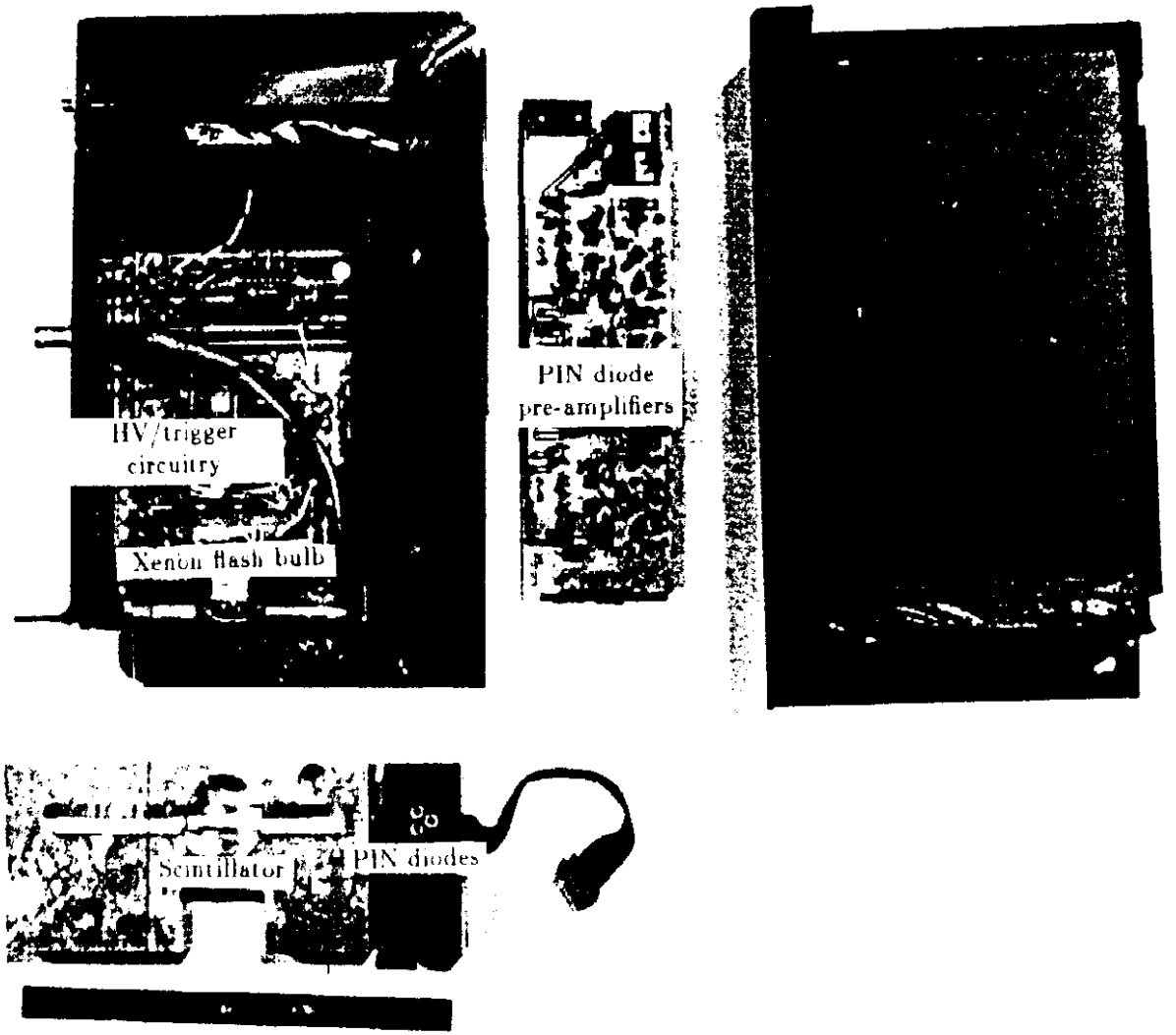
HV/trigger
circuitry
Xenon flash bulb
PIN diode
pre-amplifiers
Scintillator
PIN diodes

Fig 5

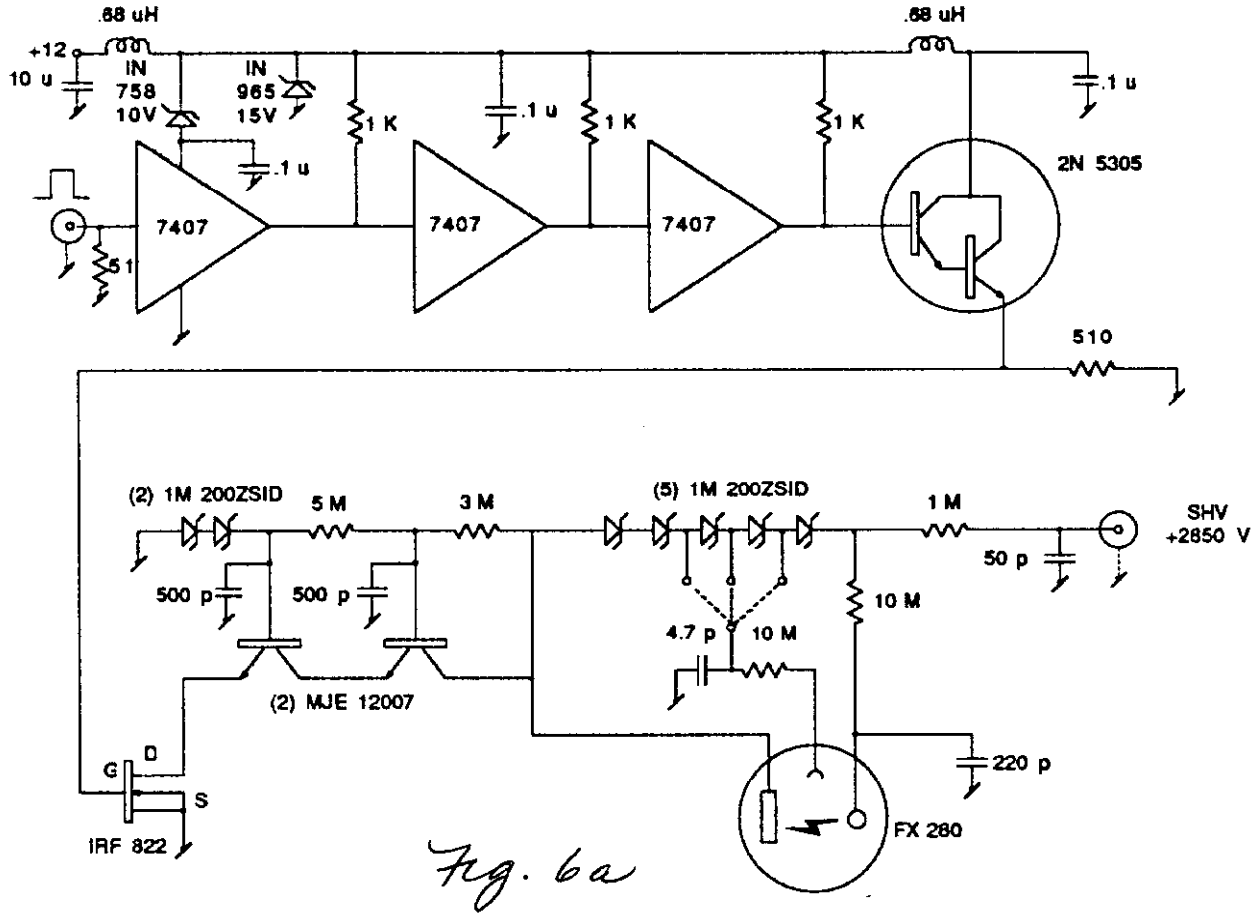
.68 uH
.68 uH
+12
10 u
IN
758
10V
IN
965
15V
1 K
.1 u
1 K
1 K
.1 u
.1 u
2N 5305
7407
7407
7407
51
510
(2) 1M 200ZSID
5 M
3 M
(5) 1M 200ZSID
1 M
SHV
+2850 V
50 p
500 p
500 p
10 M
4.7 p
10 M
(2) MJE 12007
G
D
S
IRF 822
220 p
FX 280

Fig. 6a

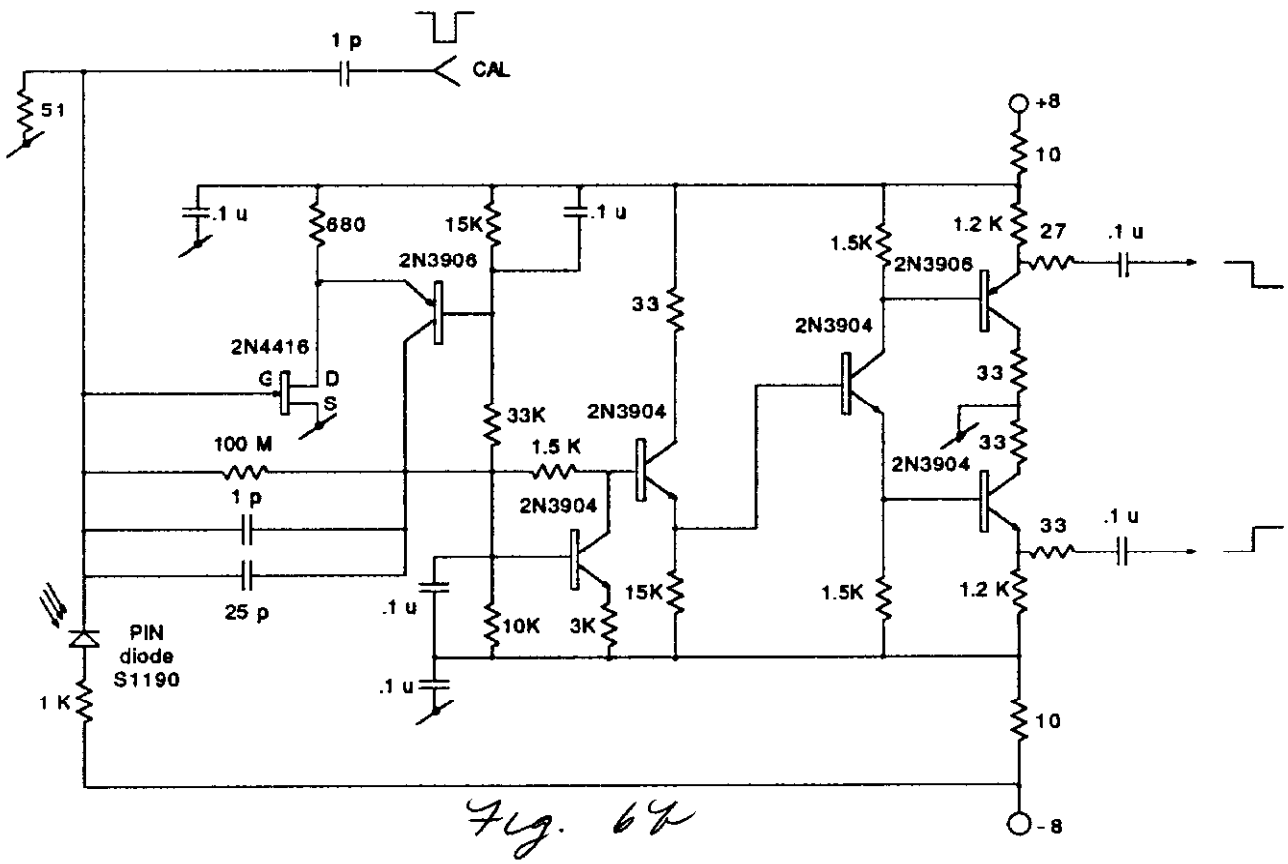
1 p
CAL
51
+8
10
.1 u
680
15K
.1 u
1.2 K
27
.1 u
1.5K
2N3906
2N3906
33
2N3904
2N4416
G
D
S
33
33K
2N3904
33
100 M
1.5 K
2N3904
1 p
2N3904
33
.1 u
25 p
.1 u
15K
1.5K
1.2 K
PIN
diode
S1190
10K
3K
.1 u
1 K
10
-8

Fig. 6b

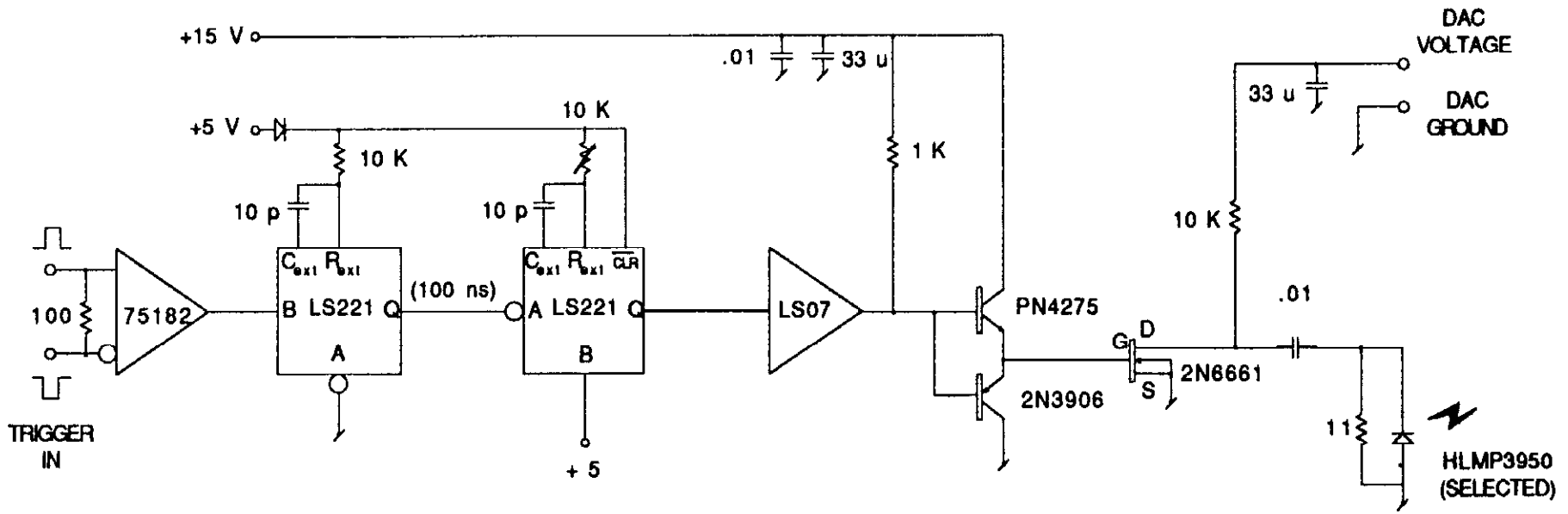
+15 V
.01
33 u
DAC VOLTAGE
33 u
DAC GROUND
+5 V
10 K
10 K
1 K
10 p
10 p
10 K
100
75182
B LS221 Q
A
(100 ns)
A LS221 Q
B
LS07
PN4275
2N3906
G
D
S
2N6661
.01
11
HLMP3950 (SELECTED)
TRIGGER IN
+ 5

Fig. 7

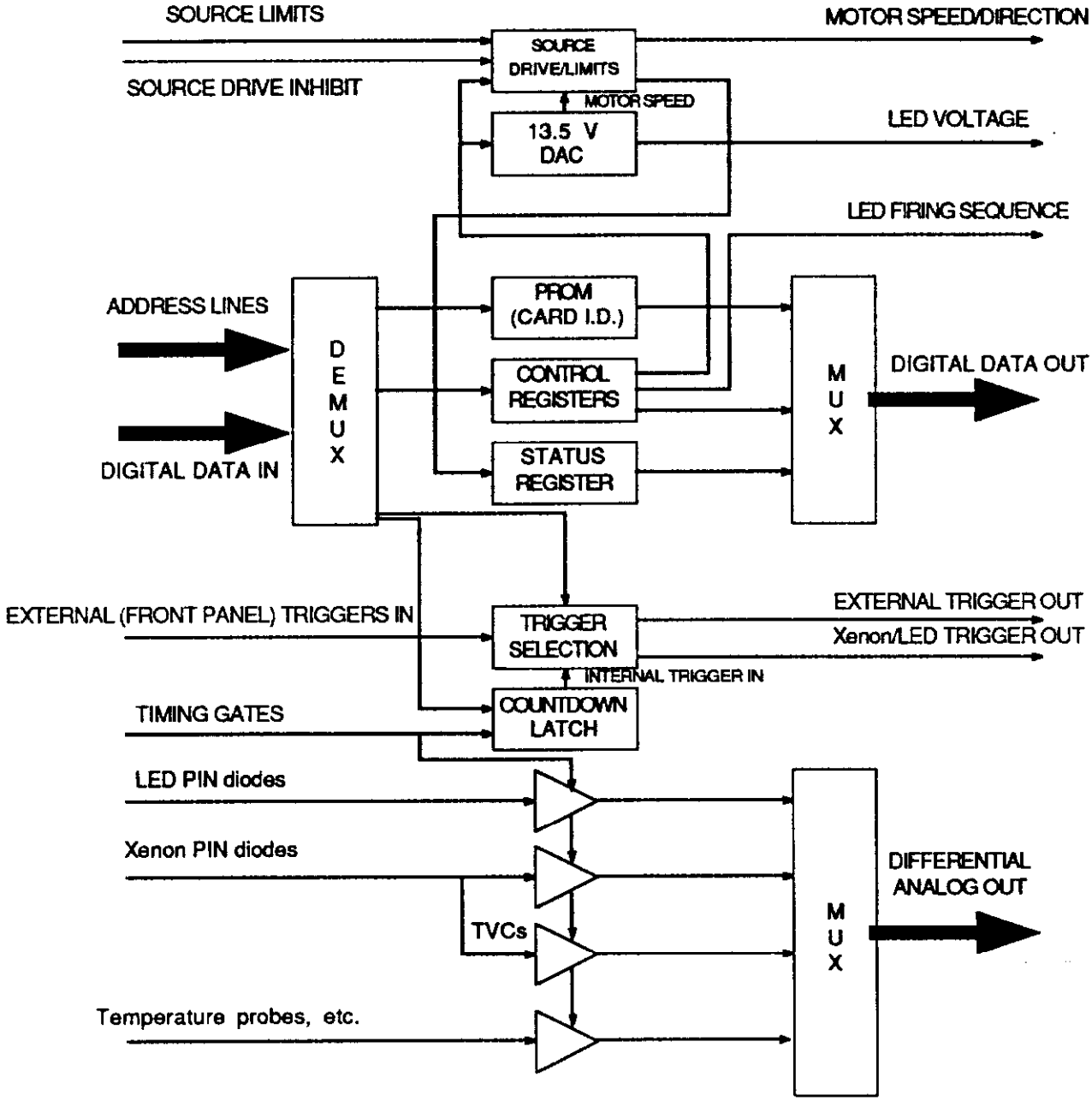
SOURCE LIMITS
SOURCE DRIVE INHIBIT
SOURCE DRIVE/LIMITS
MOTOR SPEED
13.5 V DAC
MOTOR SPEED/DIRECTION
LED VOLTAGE
LED FIRING SEQUENCE
ADDRESS LINES
DIGITAL DATA IN
DEMUX
PROM (CARD I.D.)
CONTROL REGISTERS
STATUS REGISTER
MUX
DIGITAL DATA OUT
EXTERNAL (FRONT PANEL) TRIGGERS IN
TRIGGER SELECTION
INTERNAL TRIGGER IN
EXTERNAL TRIGGER OUT
Xenon/LED TRIGGER OUT
TIMING GATES
COUNTDOWN LATCH
LED PIN diodes
Xenon PIN diodes
TVCs
Temperature probes, etc.
MUX
DIFFERENTIAL ANALOG OUT

Fig. 8

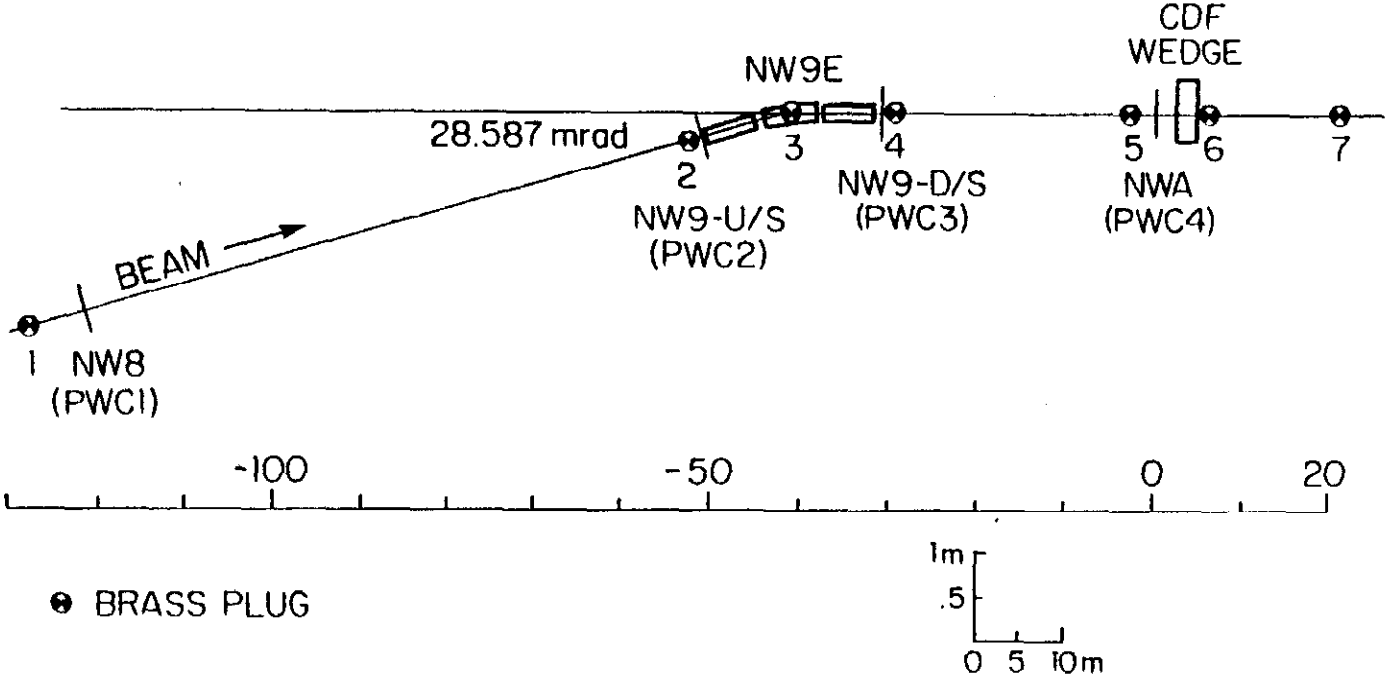
CDF
WEDGE
NW9E
28.587 mrad
1
NW8
(PWC1)
BEAM
2
NW9-U/S
(PWC2)
3
4
NW9-D/S
(PWC3)
5
6
NWA
(PWC4)
7
-100
-50
0
20
BRASS PLUG
1m
.5
0 5 10m

Fig. 9

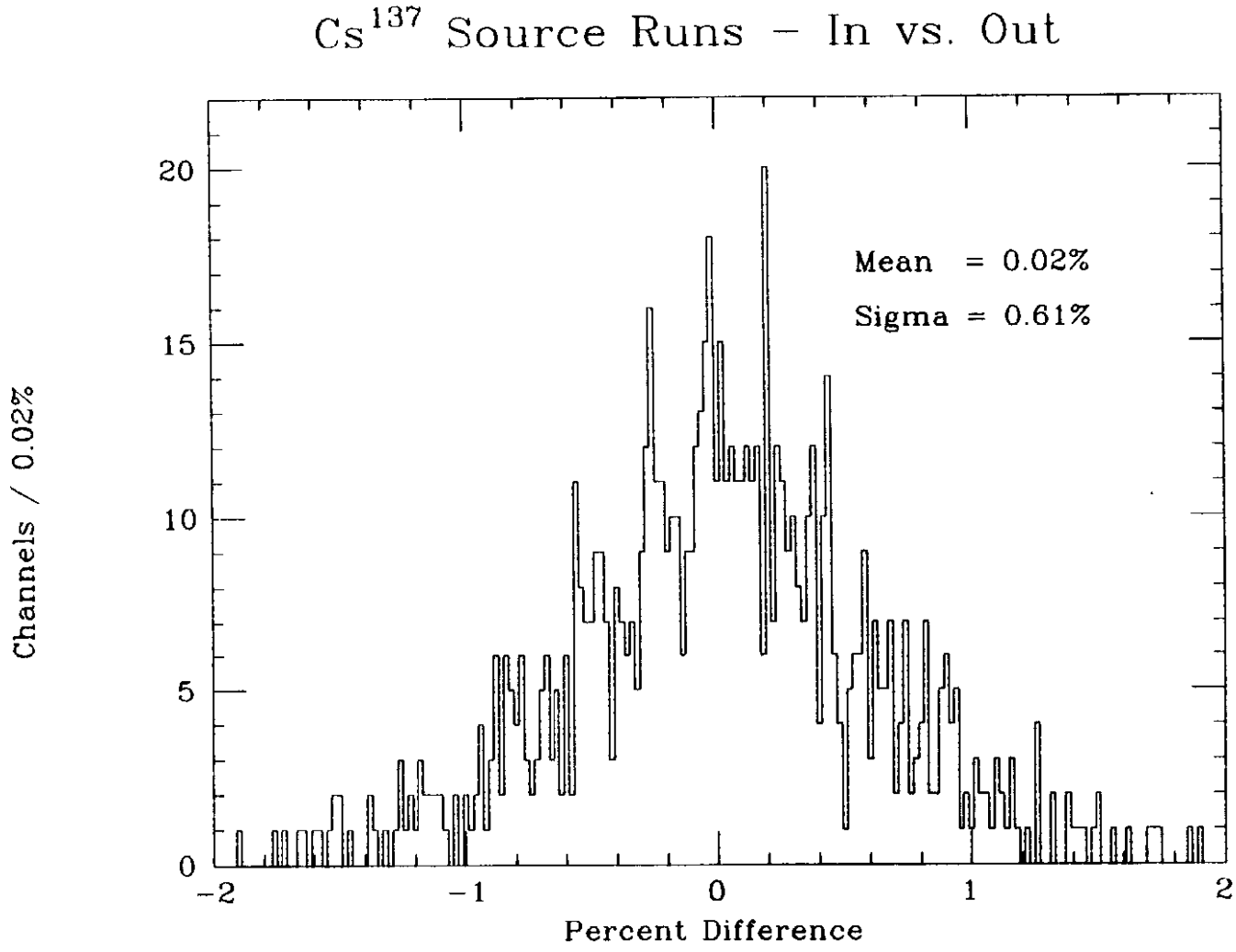
Cs^{137} Source Runs – In vs. Out
Mean = 0.02%
Sigma = 0.61%
Channels / 0.02%
Percent Difference
0
5
10
15
20
−2
−1
0
1
2

Fig. 10

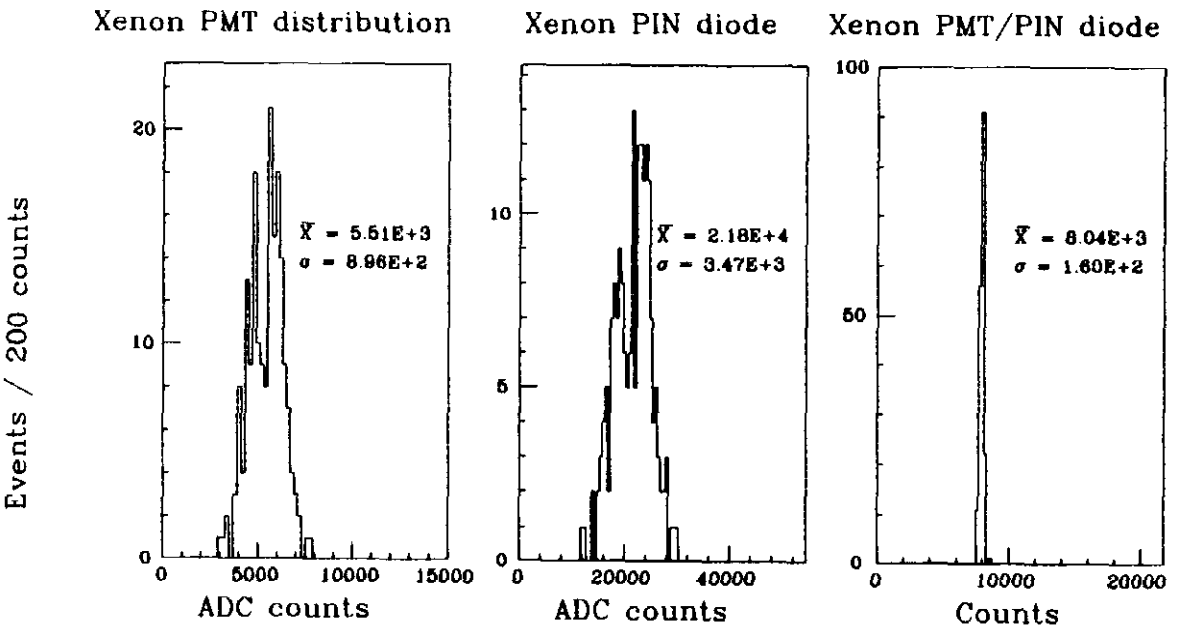
Xenon PMT distribution
Xenon PIN diode
Xenon PMT/PIN diode
Events / 200 counts
X̄ = 5.51E+3
σ = 8.96E+2
X̄ = 2.18E+4
σ = 3.47E+3
X̄ = 8.04E+3
σ = 1.60E+2
ADC counts
ADC counts
Counts

Fig. 11

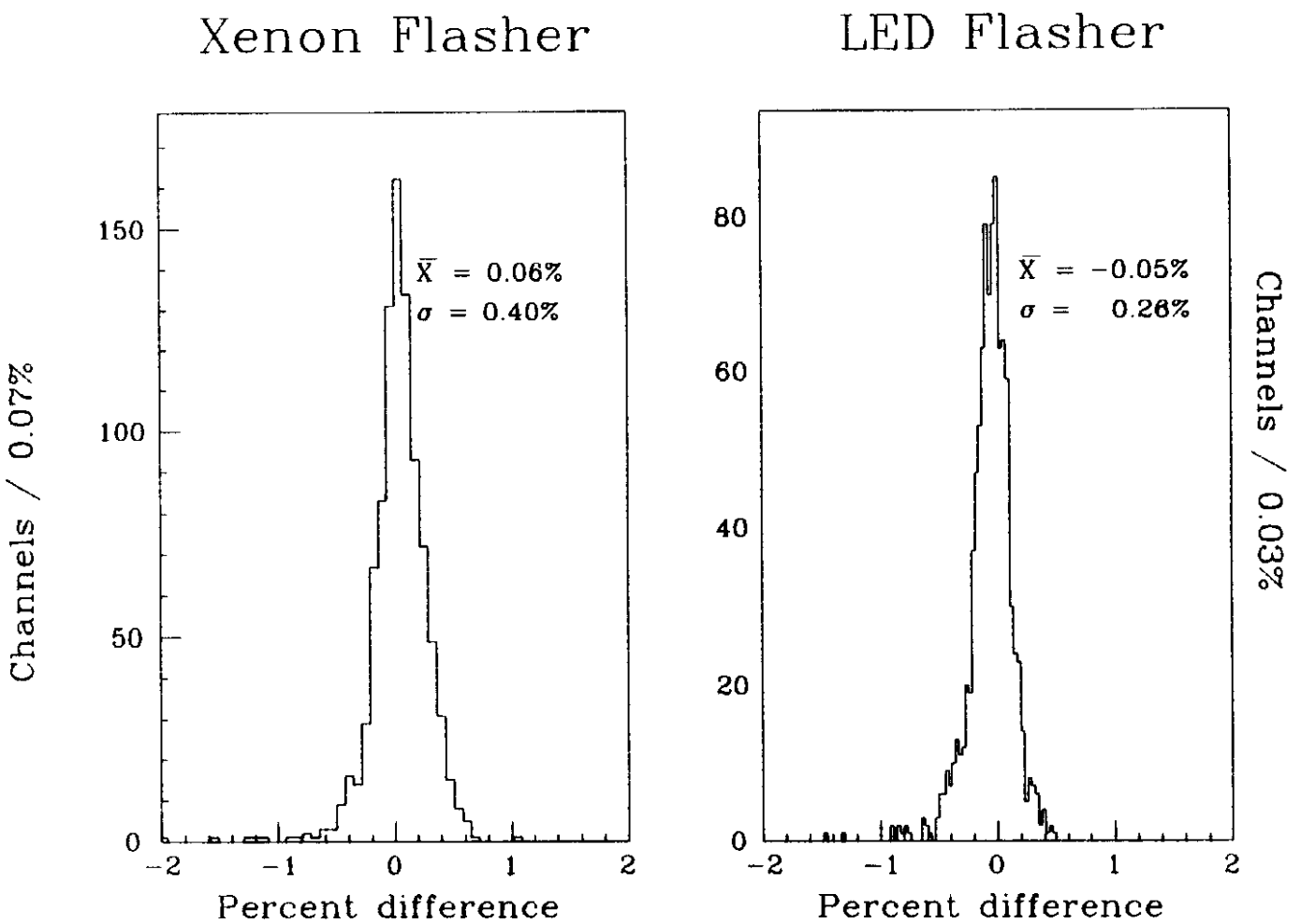
Xenon Flasher
LED Flasher
Channels / 0.07%
Channels / 0.03%
$\bar{X}$ = 0.06%
σ = 0.40%
$\bar{X}$ = −0.05%
σ = 0.26%
Percent difference
Percent difference

Fig. 12

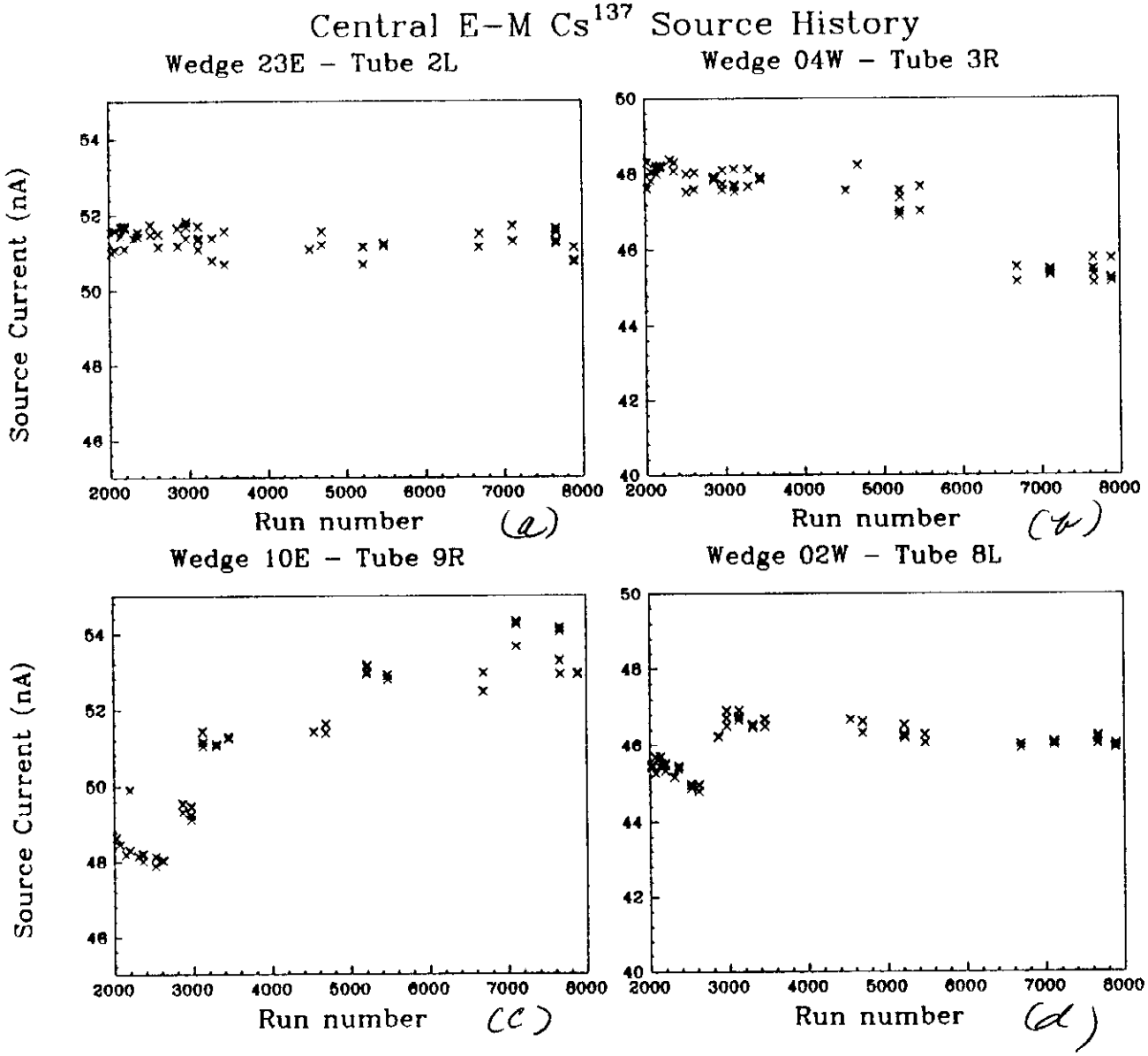
Central E-M Cs^{137} Source History
Wedge 23E - Tube 2L
Wedge 04W - Tube 3R
Wedge 10E - Tube 9R
Wedge 02W - Tube 8L
Source Current (nA)
Run number
(a)
(b)
(c)
(d)

Fig. 13

Central E-M Xenon/LED History

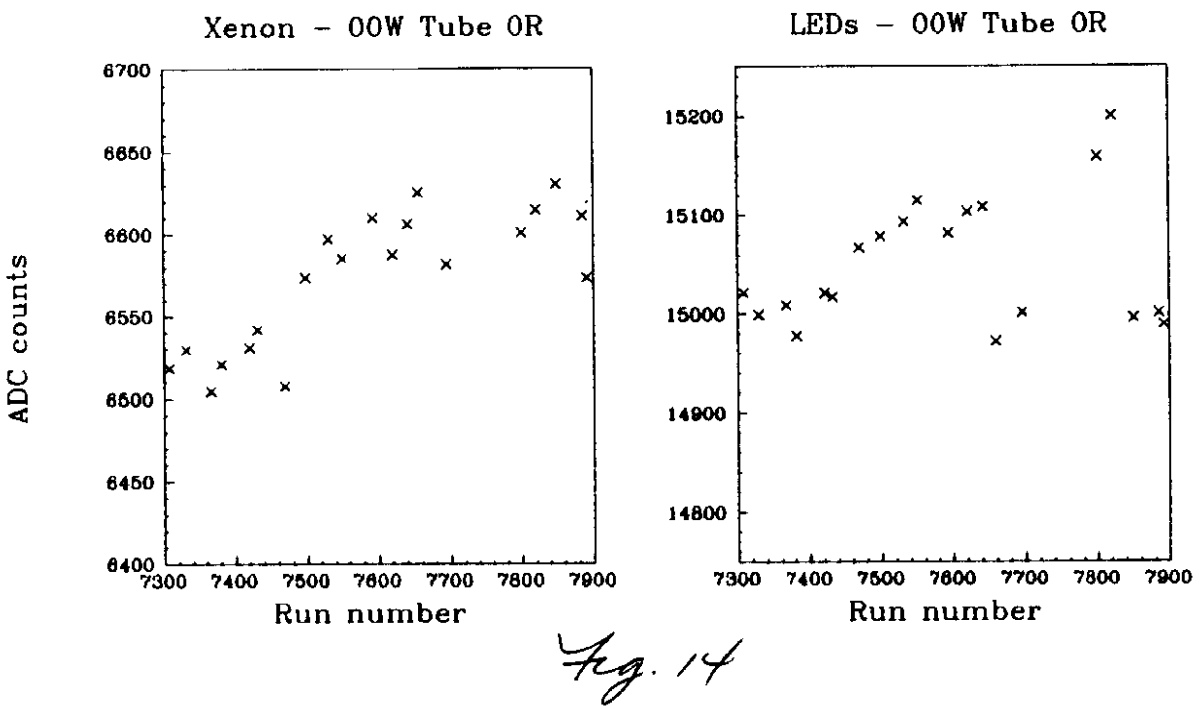

Fig. 14

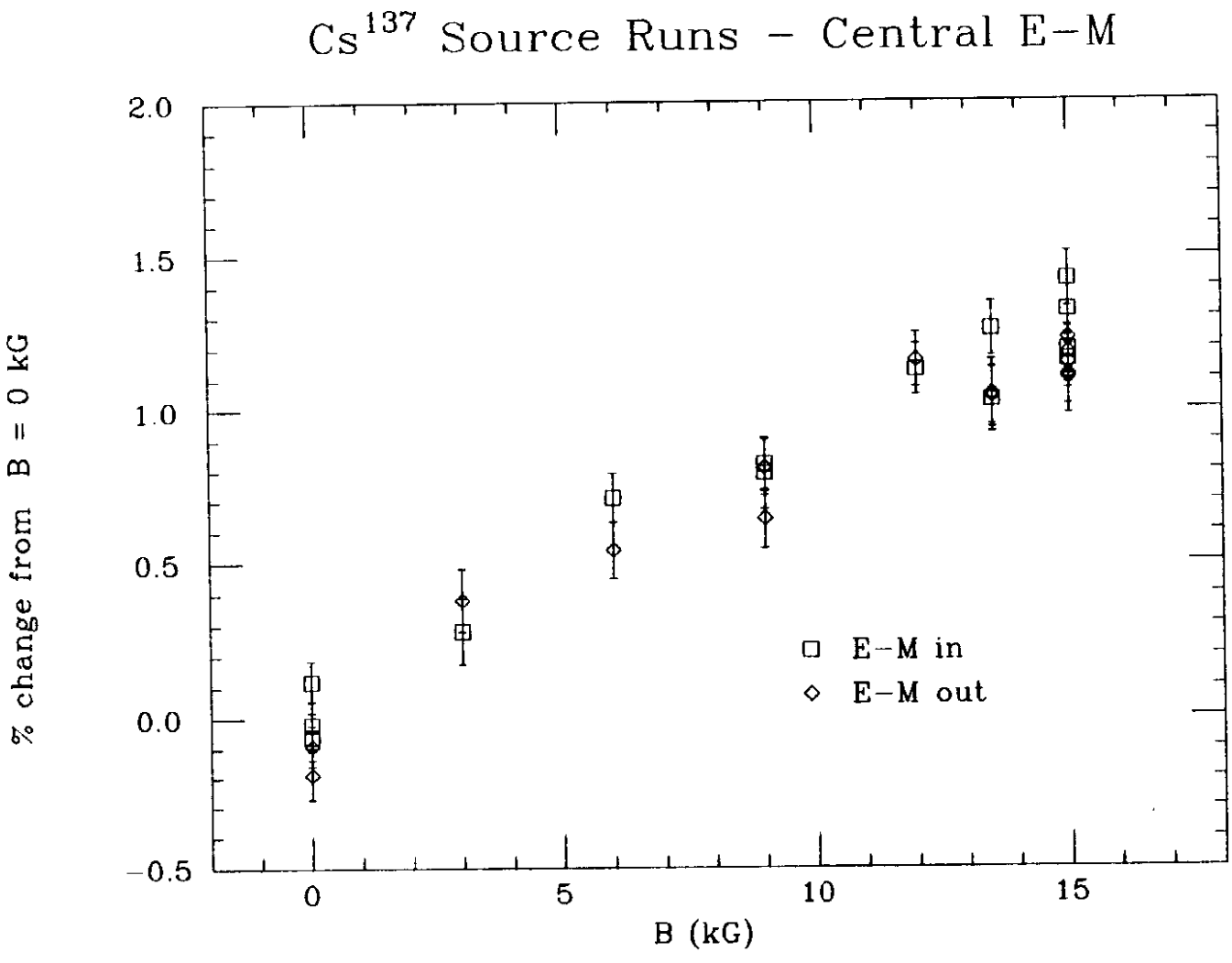
Cs137 Source Runs – Central E–M
% change from B = 0 kG
2.0
1.5
1.0
0.5
0.0
−0.5
0
5
10
15
B (kG)
E–M in
E–M out

Fig. 15

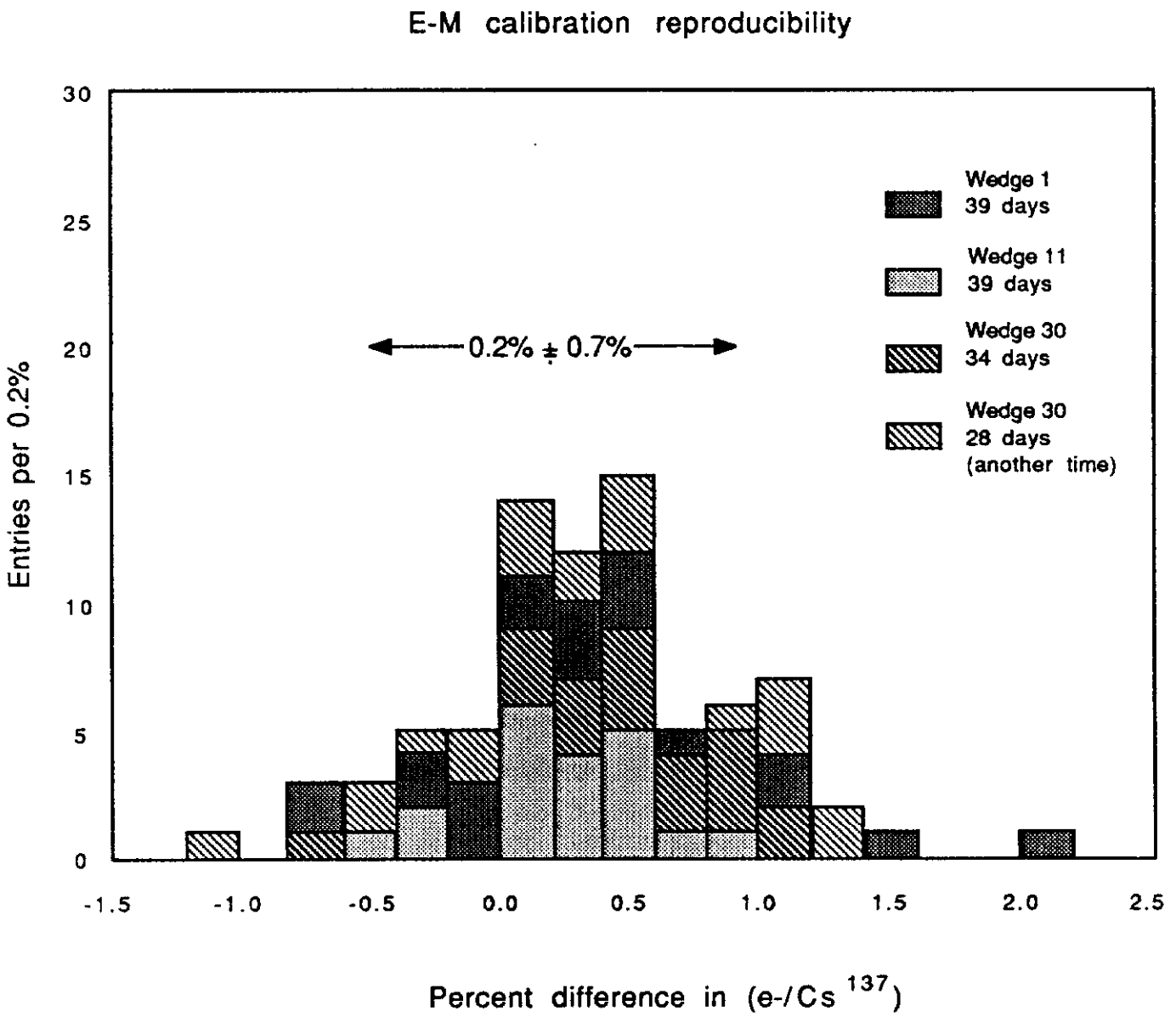
E-M calibration reproducibility
30
25
20
15
10
5
0
Entries per 0.2%
0.2% ± 0.7%
Wedge 1
39 days
Wedge 11
39 days
Wedge 30
34 days
Wedge 30
28 days
(another time)
-1.5
-1.0
-0.5
0.0
0.5
1.0
1.5
2.0
2.5
Percent difference in (e-/Cs 137)

Fig. 16

Central E–M Gain Variations

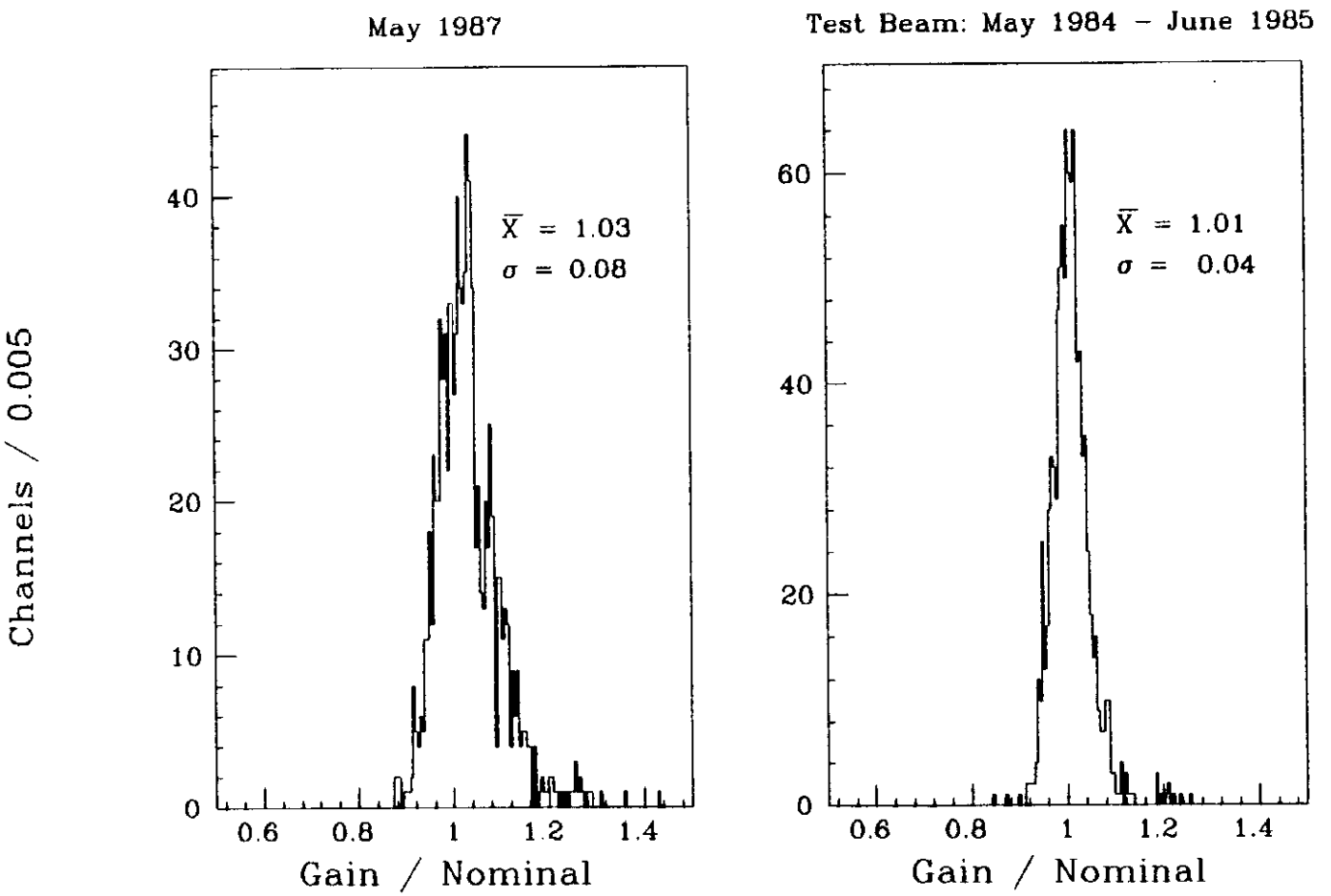

(a) Fig. 17 (b)

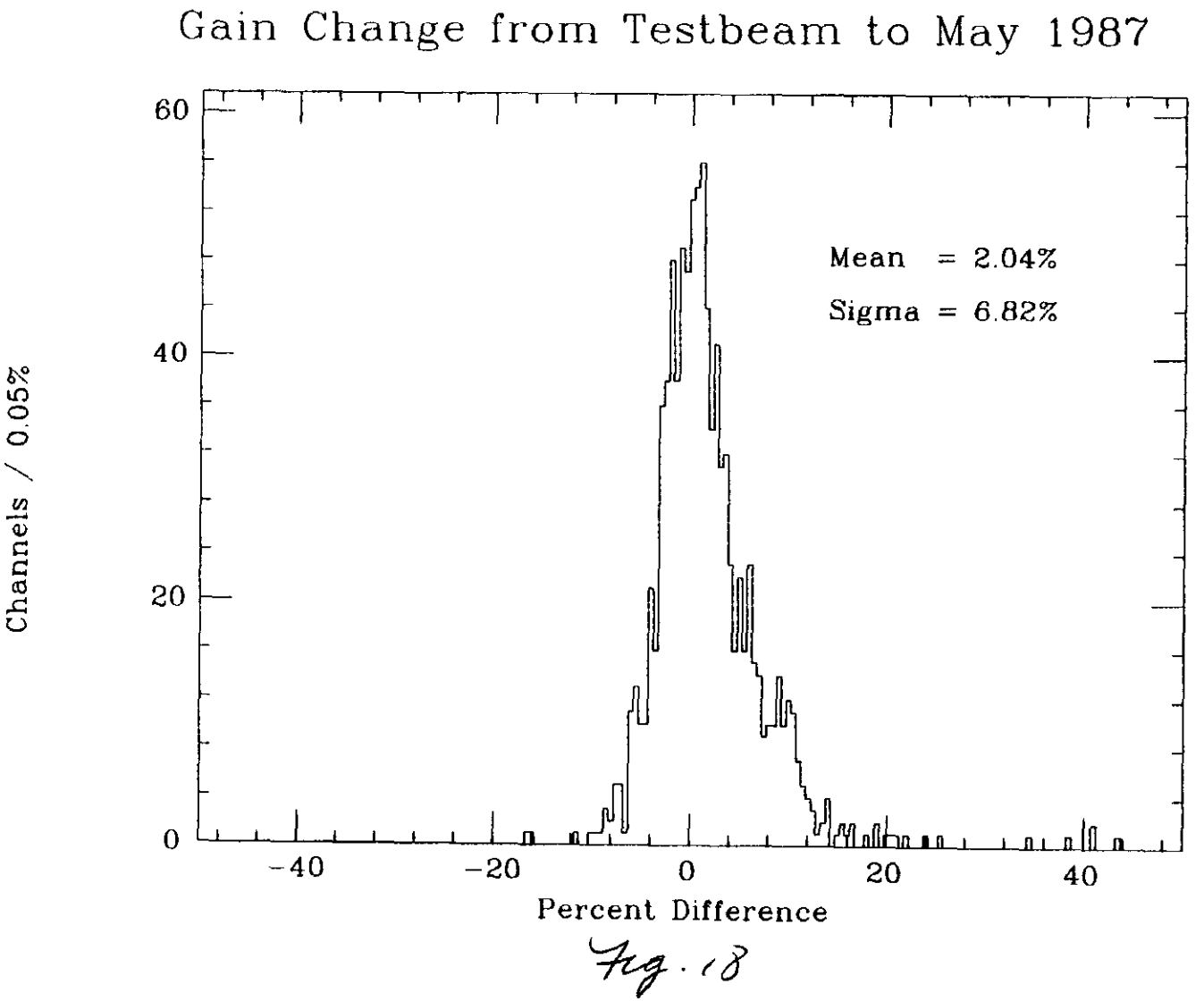
Gain Change from Testbeam to May 1987
Channels / 0.05%
60
40
20
0
Mean = 2.04%
Sigma = 6.82%
-40
-20
0
20
40
Percent Difference

Fig. 18